



Partitioning the solar radiant fluxes in forest canopies in the presence of snow

B. Pinty,¹ T. Lavergne,¹ T. Kaminski,² O. Ausedat,¹ R. Giering,² N. Gobron,¹ M. Taberner,¹ M. M. Verstraete,¹ M. Voßbeck,² and J.-L. Widlowski¹

Received 25 June 2007; revised 2 October 2007; accepted 29 October 2007; published 20 February 2008.

[1] The main goal of this study is to help bridge the gap between available remote sensing products and large-scale global climate models. We present results from the application of an inversion method conducted using both MODerate resolution Imaging Spectroradiometer (MODIS) and Multiangle Imaging SpectroRadiometer (MISR) derived broadband visible and near-infrared surface albedo products. This contribution is an extension of earlier efforts to optimally retrieve land surface fluxes and associated two-stream model parameters (Pinty et al., 2007). It addresses complex geophysical scenarios involving snow occurrence in mid and high-latitude evergreen and deciduous forest canopy systems. The detection of snow during the winter and spring seasons is based on the MODIS snow product. This information is used by our package to adapt the prior values, specifically the maximum likelihood and width of the 2-D probability density functions (PDF) characterizing the background conditions of the forest floor. Our results (delivered as a Gaussian approximation of the PDFs of the retrieved model parameter values and radiant fluxes) illustrate the capability of the inversion package to retrieve meaningful land vegetation fluxes and associated model parameters during the year, despite the rather high temporal variability in the input products, in large part due to the occurrence of snow events. As a matter of fact, most of this temporal variability, as well as the small differences between the MODIS and MISR broadband albedos, appear to be largely captured by the albedo of the forest canopy background.

Citation: Pinty, B., T. Lavergne, T. Kaminski, O. Ausedat, R. Giering, N. Gobron, M. Taberner, M. M. Verstraete, M. Voßbeck, and J.-L. Widlowski (2008), Partitioning the solar radiant fluxes in forest canopies in the presence of snow, *J. Geophys. Res.*, 113, D04104, doi:10.1029/2007JD009096.

1. Introduction

[2] An accurate knowledge of the land processes controlling the partition of solar radiant flux between the vegetation and the underlying soil layer is required to improve simulations of the soil-vegetation-atmosphere exchanges at various space and timescales of interest for climate, numerical weather prediction as well as carbon cycle models [e.g., Pitman, 2003]. The energy absorbed in the vegetation layer is used to drive processes such as evapotranspiration, photosynthesis and carbon assimilation, while the remaining fraction available in the underlying soil controls evaporation, snowmelting and temperature related processes [e.g., Dickinson, 1983; Avissar and Verstraete, 1990; Sellers et al., 1997; Viterbo and Betts, 1999]. All these processes are ultimately linked to fluxes such as the latent and sensible heat fluxes at the top of the vegetation canopy and the ground heat flux. The relevance of these fluxes with respect

to various geophysical issues largely depend on space and timescales of concern [e.g., Verstraete, 1989; Betts, 2007].

[3] Monitoring the environment at a continental or global scale, over periods of multiple years, requires access to reliable and accurate geophysical quantities and satellite remote sensing is the only technology currently available to provide consistent data at these scales. These quantities include the fraction of the radiant flux scattered by the surface at the top of the canopy, and in particular the albedo in the broadband visible (0.3–0.7 μm) and near-infrared (0.7–3.0 μm) spectral domains. These estimates, provided at various spatial resolutions, are thus fully relevant to applications requiring an accurate and precise understanding and/or simulations of the surface energy balance at the surface upper boundary condition, irrespective of whether this step is achieved via a process-based radiation transfer scheme [Dickinson et al., 1986; Sellers, 1985] or a look-up-table based approach.

[4] In any case, land surface radiation transfer schemes are needed to partition the solar radiation between the vegetation and soil as a function of parameters such as the amount, density and optical properties of leaves, as well as the properties of the topsoil/background layer. The accuracy of the solutions to this radiation partitioning problem depends

¹European Commission, DG Joint Research Centre, Institute for Environment and Sustainability, Global Environment Monitoring Unit, Fermi, Italy.

²FastOpt, Hamburg, Germany.

on the performance of the selected radiation transfer scheme, the availability of input remote sensing flux products and the quality of the retrieval procedure which makes optimal use of the available prior information. Such a retrieval procedure has been devised and its performance is documented in detail in *Pinty et al.* [2007] and *Lavergne et al.* [2006]. Evidence has been collected from simulation and inversion exercises, as well as a set of applications performed over selected midlatitude Earth Observing System (EOS) validation sites. These applications exploit operational surface albedo products from the MODerate resolution Imaging Spectroradiometer (MODIS) [*Schaaf et al.*, 2002], the Multiangle Imaging Spectroradiometer (MISR) [*Martonchik et al.*, 1998] on board the Terra platform and the Fraction of Absorbed Photosynthetically Active Radiation (FAPAR) product derived from the Sea-viewing Wide Field-of-view Sensor (SeaWiFS) [*Gobron et al.*, 2006].

[5] This paper capitalizes on results from previous studies, as discussed in [*Pinty et al.* [2007]], and more specifically addresses the issue of the partitioning of solar radiation between the vegetation and soil layers in the more difficult but rather relevant case of tall spatially heterogeneous (3-D) forest canopies subject to significant changes in their background properties as a result, for instance, of the occurrence of snow in the winter and spring seasons. Such geophysical situations are quite challenging because most forest canopies exhibit a significant and unresolved internal variability (along the horizontal and vertical directions) of their properties such as, for instance, the leaf area density. Furthermore, the occurrence and melting of snow implies drastic changes in the radiative properties of the background. Meanwhile, these changes offer challenging conditions to further test the Joint Research Centre Two-stream Inversion Package (JRC-TIP) given that the main properties of the vegetation layer are expected to exhibit small (for environment dominated by evergreen forests) or smooth variations during the year (in the case of deciduous systems), unlike the albedo products which are quite sensitive to these drastic changes occurring on the forest floor.

[6] Section 2 reviews the four main elements required to achieve the proposed application, namely 1) the forward radiation transfer model, 2) the inversion methodology, 3) the remote sensing surface albedo data sets and 4) the specification of prior information. Results from a series of applications are shown and discussed in section 3. Time series of the vegetation canopy parameters and associated radiant fluxes estimated over different forest systems from the JRC-TIP are first presented in section 3.1. Our retrieved FAPAR values are then compared in section 3.2 with those available operationally from various agencies. Finally, the consequences of the differences in the MODIS and MISR surface albedo products on the surface retrievals are assessed in section 3.3.

2. Summary of the Inversion Scheme

2.1. The Two-Stream Forward Model

[7] *Pinty et al.* [2006a] developed and validated a new version of a two-stream model suited for the simulation of solar radiant fluxes scattered by, transmitted through and absorbed in a vegetation canopy made up of bi-Lambertian leaves, possibly exhibiting a preferred orientation. The bi-

Lambertian leaf scattering property is such that the fraction of radiation that is not absorbed is scattered as a cosine distribution around the leaf normal vectors. The top and bottom boundary conditions are specified by the downwelling direct and diffuse radiant fluxes and the albedo of the background, respectively. This model is constructed from dedicated solutions to three separate problems involving 1) the scattering by the vegetation layer only, identified as the black-background contribution, 2) the flux transmitted directly through the vegetation layer involving only the background, that is the black-canopy contribution and finally 3) the contribution to the upward and downward scattered and transmitted fluxes involving multiple interactions between both the vegetation layer and its underlying background. Specific efforts were made to minimize the computational burden associated with the implementation and maintenance of this scheme in host models such as climate and numerical weather prediction models.

[8] This 1-D model provides a solution to the black background problem which follows the two-stream formulation established originally by [*Meador and Weaver* [1980]]. It ensures the correct balance between the scattered, transmitted and absorbed radiant fluxes for structurally homogeneous as well as heterogeneous canopies provided that, in the latter case, effective instead of true state variables are adopted. Indeed, as demonstrated by *Pinty et al.* [2004a, section 3.3], a solution to a 3-D flux problem satisfying the conditions imposed by a “radiatively independent volume” can always be achieved using a 1-D representation, but at the cost of parameterizing the true state variables. It thus implies that scattered flux quantities or albedos derived from medium resolution sensors can be interpreted in inverse mode with a 1-D model to partition the radiation between the vegetation and soil layers. The performance of this 1-D model to generate accurate fluxes has been established against solutions delivered by 3-D Monte-Carlo models under standard and extreme environmental conditions including conservative scattering [see *Pinty et al.*, 2004a; *Widlowski et al.*, 2006].

[9] These effective variables are, a spectrally invariant quantity, namely the Leaf Area Index (LAI) and, spectrally dependent parameters that are the leaf single scattering albedo $\omega_l = r_l + t_l$ and the ratio $d_l = r_l/t_l$ (identified here as the asymmetry factor) where r_l and t_l correspond to the leaf reflectance and transmittance, respectively. The albedo of the background, r_g , is itself defined as the true (by contrast to effective) value and retrieved as such. The effective LAI value expresses the capability of the vegetation layer to intercept direct radiation, and is thus associated with the probability distribution function of the canopy gaps. This quantity is generally measured in the field with standard optical devices [e.g., *Rich*, 1990; *Gower and Norman*, 1991; *Jonckheere et al.*, 2004]. Accordingly, the two main parameters controlling the flux partitioning, i.e., the effective LAI and the true background albedo, can be estimated from in situ measurements and this offers a practical means to evaluate the quality of the retrievals delivered by the inversion procedure.

2.2. Formalism of the Inverse Problem

[10] We adopted a rather generic formulation of the inverse problem [e.g., *Tarantola*, 1987; *Enting et al.*,

1995] in which the solutions combine all available information, i.e., the prior knowledge on the PDFs of the model parameters \mathbf{X} , the measurements \mathbf{d} (here the remote sensing derived surface albedo values), and the constraint provided by the model $M(\mathbf{X})$ (e.g., the two-stream model outlined in section 2.1). These solutions are delivered as an approximate characterization of the PDFs of the retrieved model parameter values. Under some regularity assumptions [Pinty *et al.*, 2007, section 2.2], these solutions derived in the space of the model parameters can be approximated by a multidimensional Gaussian PDF:

$$P(\mathbf{X}) \approx \exp\left(-\frac{1}{2}(\mathbf{X} - \mathbf{X}_{post})^T \mathbf{C}_{X_{post}}^{-1} (\mathbf{X} - \mathbf{X}_{post})\right) \quad (1)$$

where \mathbf{X}_{post} represents the mean of $P(\mathbf{X})$, $\mathbf{C}_{X_{post}}$ is the covariance matrix of the posterior uncertainties on the retrieved model parameters. The diagonal elements of this matrix are given by the variances $\sigma_{X_{post}}^2$ of the marginal PDFs along each model parameter axis. Its off-diagonal elements are covariances quantifying the bindings in the uncertainties on retrieved model parameters. The superscript T denotes the matrix transpose operator. \mathbf{X}_{post} is the location in the space of model parameters which minimizes the cost function $J(\mathbf{X})$ expressed as follows:

$$J(\mathbf{X}) = \frac{1}{2} \left[(M(\mathbf{X}) - \mathbf{d})^T \mathbf{C}_d^{-1} (M(\mathbf{X}) - \mathbf{d}) + (\mathbf{X} - \mathbf{X}_{prior})^T \mathbf{C}_{X_{prior}}^{-1} (\mathbf{X} - \mathbf{X}_{prior}) \right] \quad (2)$$

where \mathbf{C}_d is the covariance matrix of uncertainties in the measurement set, which also accounts for the uncertainty due to model error, and $\mathbf{C}_{X_{prior}}$ is the Gaussian uncertainty matrix associated with the prior knowledge on the model parameters, i.e., the PDFs of the prior values. The posterior uncertainties on the model parameters are estimated from an analysis of the curvature of $J(\mathbf{X})$ and the covariance matrix $\mathbf{C}_{X_{post}}$ is further exploited to estimate the PDFs of the radiant flux quantities that the model $M(\mathbf{X})$, i.e., the two-stream model in this application, is able to simulate. The PDFs of all the radiant fluxes that can be simulated by the model are approximated by the Gaussian PDF with mean $M(\mathbf{X}_{post})$ and covariance of uncertainties (assuming a perfect model) given by:

$$\mathbf{C}_{post}^{Flux} = \mathbf{G} \mathbf{C}_{X_{post}} \mathbf{G}^T \quad (3)$$

where \mathbf{G} denotes the Jacobian matrix of $M(\mathbf{X})$ at minimum, i.e., $\mathbf{G} = \partial M(\mathbf{X}_{post}) / \partial \mathbf{X}$ with a linearization around the mean values \mathbf{X}_{post} . In practice, the compiler tool Transformation of Algorithms in C++ (TAC++) [Giering and Kaminski, 1998] available from FastOpt (<http://www.FastOpt.com/>) has been used to generate the software for the adjoint, tangent linear and Hessian codes of the cost function $J(\mathbf{X})$. Information regarding the computer efficiency of the JRC-TIP are given by Pinty *et al.* [2007, section 3].

2.3. Measurement Set

[11] The measurement set considered in the series of applications discussed in this paper essentially includes the two broadband visible (identified with subscript 1)

and near-infrared (identified with subscript 2) surface albedo products associated with both the MODIS (collection 4) and MISR (collection 6 from version 17 of the operational processor) instruments on board the Terra platform. More precisely, those products are Bi-Hemispherical Reflectance (BHR) values that are intrinsic surface properties (this product is called ‘white sky’ albedo [Schaaf *et al.*, 2002]) and only those delivered with good confidence levels (Quality Assessment flag values of 0 and 1) are considered here. Surface albedo quantities similar to those from MODIS, i.e., broadband integrated BHRs, were generated from the MISR retrieved surface anisotropy parameters following the procedure outlined by Pinty *et al.* [2007, section 4]. Note, however, that due to the sequential time accumulation approach, the MODIS surface albedo products are representative of a 16-day period while the MISR products are derived from data acquisition at the time of overpass.

[12] The covariance matrix associated with these measurements, \mathbf{C}_d , is assumed diagonal and associated with the combined uncertainty in the measurements and model error. Standard deviation values of 5% of the estimated values for the fraction of reflected spectral fluxes in the visible, R_1 , and near-infrared, R_2 , domains are specified in our baseline set up.

[13] Time series of these 1 km resolution remote sensing products available for year 2005 over instrumented forest sites (see, for instance, <http://www.fluxnet.ornl.gov/> and <http://www.carboeurope.org/>) exhibiting a variety of vegetation phenological cycles (like those typically associated with high and midlatitude evergreen or deciduous needle and broadleaf forests) and the very likely occurrence of snow during the winter and spring seasons have been selected (see Table 1). All these sites sample a radiation transfer regime associated with a significant 3-D internal variability, of the leaf area density for instance, which finally controls the domain/pixel-averaged radiant fluxes [see Gobron *et al.*, 2006 for detailed discussions].

2.4. Prior Knowledge on Model Parameters

[14] The specification of prior information on the model parameters transforms an ill-posed into a well-posed inverse problem (see equation (2)). Given that the objective of solving the inverse problem is to increase our current knowledge on the system on the basis of the observations included in the measurements set, the quality of the prior information must be evaluated and specified with great care: imposing excessively stringent conditions on the width of the PDFs of the prior parameters implies that little knowledge will be gained from the inversion, while setting too loose specifications translates into high posterior uncertainties.

[15] The strategy adopted here favors a generic set up of the prior values to limit the dependency with respect to specific land cover or biome types. It acknowledges 1) a rather limited knowledge on LAI, i.e., expressed by a large variance value equal to 25.0 on the diagonal of the covariance matrix, which may exhibit large spatial and temporal variability along the year, 2) an explicit correlation between samples of the soil albedo values in the visible and near-infrared domains, usually referred to as the ‘soil line’ concept [see Chi, 2003, for a review] that can vary in the presence of snow and, 3) the overall ‘greenness’ of the

Table 1. Identification and Main Characteristics of the Selected Sites^a

Field site Identification	Geographical Coordinates	Dominant Vegetation Type and Tree Species
NSAOBS (Boreas site, Canada)	55.88007°N 98.48139°W	evergreen needleleaf black spruce forest
METL (Metolius, USA)	44.437189°N 121.566756°W	evergreen needleleaf young ponderosa pine forest
CHEQCenter (Park Falls, USA)	45.945404°N 90.272475°W	mixed deciduous conifer forest
YAKUTSKspas (Spasskya Pad, Russia)	62.255000°N 129.618800°E	deciduous needleleaf larch forest
HESSE (France)	48.67422°N 7.064617°E	deciduous broadleaf beech forest
Harv (Harvard forest, USA)	42.538259°N 72.171378°W	deciduous broadleaf emlock forest

^aBased on information collected on various web sites, <http://www.fluxnet.ornl.gov/> and <http://www.carboeurope.org/>.

needles or leaves, i.e., relatively small values on the variance, in both the visible and near-infrared domains, associated with the mean values of the PDFs of the effective single scattering albedo. The corresponding mean values have been estimated from an ensemble of measured [Hosgood *et al.*, 1995] and modeled [Jacquemoud and Baret, 1990] leaf optical properties; they were further modified to best account for the overall effects on the domain-averaged radiant fluxes, of needle clumping into shoots, shoots or leaves clumping into crowns as well as the presence of woody elements in the canopy [Rautiainen *et al.*, 2004; Pinty *et al.*, 2004a]. In the specific cases dedicated to the assessment of the contributions due to the ‘green’ elements of the canopy only, the inversion package is operated using prior values corresponding to the so-called ‘green’ leaf scenario.

[16] Table 2 indicates the mean values \mathbf{X}_{prior} (estimated after spectral weighting by the extra terrestrial solar irradiance for the spectrally dependent parameters) and associated standard deviations $\sigma_{X_{prior}}$ used to set the diagonal of the prior covariance matrix $\mathbf{C}_{X_{prior}}$ at wavelengths λ_1 and λ_2 corresponding to the broadband visible and near-infrared spectral domains, respectively. The level of correlation imposed on the uncertainties of the background albedos are given as footnotes of Table 2.

[17] Figure 1 provides a graphical representation of this prior information on the spectrally variant parameters, namely the leaf single scattering albedo and the background conditions. The mean values are identified by the crosses and the ellipses encompass the 1.5σ uncertainty regions of the corresponding PDFs [Lavergne *et al.*, 2006, appendix G]. Measurements of a variety of leaves and needles, bare soils and snow are also reported with different symbols. It is noteworthy that the spectral relationship between the mean soil albedo values changes drastically with the occurrence of snow. Indeed, in the latter instance, the visible values exceed those estimated in the near-infrared domain, thus displaying the straightforward signature of such events. Note that the prior knowledge adopted in presence of snow has been established using a linear weighting of pure snow and relatively dark bare soil fractions. Uncertainties on all model-parameters are pairwise uncorrelated except for the background albedos. Correlation values for the latter are listed in Table 2.

[18] The inversion also makes use of the operational MODIS snow cover product. Depending on the value of this snow indicator, the inversion is performed with different sets of background albedo conditions, switching from bare soil to snow-like conditions (see Figure 1). All inversions were performed in static mode at a single time of observation (representative of the 16-day MODIS accumu-

lation time period), i.e., without coupling in the temporal domain. The MODIS snow product, identified as MOD10A2 (version 4), corresponds to a 8-day composite period (see, for instance, <http://nsidc.org/>) and is based on a set of criteria using the Normalized Difference Snow Index [Hall *et al.*, 1998]. This information is delivered at 500 m spatial resolution and, in the present application, the products were thus re-mapped using a nearest neighbor technique for all studied sites. The same re-mapping technique was used for the 1 km resolution MODIS and MISR surface albedo values.

3. Results

[19] The flexibility and potential offered by the inversion package outlined in the previous section allows us generating a large amount of internally consistent information. The results reported here have been selected to illustrate and document the performance of the JRC-TIP in various instances. The figures shown in this section exhibit the values of model parameters retrieved after inversion, whenever they are physically meaningful, i.e., within the domain defined by their possible range of variations (between 0 and 1, for instance). In the few cases when the inversion leads to negative posterior values, these results are ignored, because they obviously indicate that the information in the priors, the observations, and the model are inconsistent.

[20] The first subsection analyses the temporal variations during year 2005 of the retrieved 2-stream model parameters and the fluxes absorbed in the vegetation and the

Table 2. Mean Values \mathbf{X}_{prior} and Associated Standard Deviations $\sigma_{X_{prior}}$ Used to set the Diagonal of the Prior Covariance Matrix $\mathbf{C}_{X_{prior}}$, λ_1 and λ_2 Correspond to the Broadband Visible and Near-Infrared Spectral Domains, Respectively, $\omega_f(\lambda_{1,2})$, $d_f(\lambda_{1,2})$ and $r_g(\lambda_{1,2})$ Refer to the Single Scattering Albedo, Asymmetry Factor and Background Albedo, Respectively

Variable Identification	\mathbf{X}_{prior}	$\sigma_{X_{prior}}$
LAI	1.5000	5.0
$\omega_f(\lambda_1)$	0.1700 and 0.1300 ^a	0.1200 and 0.0140 ^a
$d_f(\lambda_1)$	1.0000	0.7000
$r_g(\lambda_1)$	0.1000 ^b and 0.35 ^c	0.0959 ^b and 0.346 ^c
$\omega_f(\lambda_2)$	0.7000 and 0.7700 ^a	0.1500 and 0.0140 ^a
$d_f(\lambda_2)$	2.0000	1.5000
$r_g(\lambda_2)$	0.1800 ^b and 0.50 ^c	0.2000 ^b and 0.25 ^c

^aValues associated with the ‘green’ leaf scenario.

^bValues adopted for the bare soil case with a correlation factor, between the two spectral domains, of 0.8862 set in $\mathbf{C}_{X_{prior}}$.

^cValues adopted under occurrence of snow with a correlation factor, between the two spectral domains, of 0.8670 set in $\mathbf{C}_{X_{prior}}$.

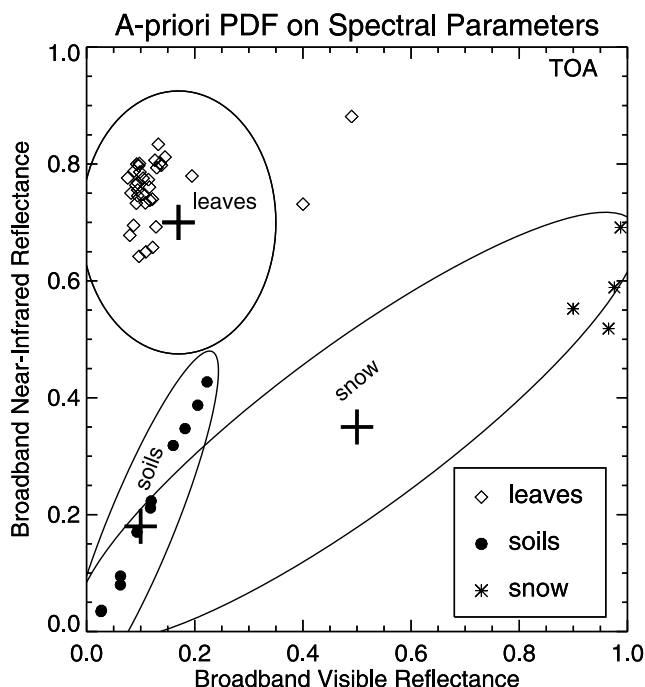


Figure 1. Graphical representation in the visible and near-infrared plane of the prior information on the spectrally variant parameters, namely the leaf single scattering albedo and the background conditions. The mean values of the PDFs are identified by the crosses (in bold) and the surrounding ellipses encompass the 1.5σ uncertainty regions of the corresponding PDFs. The different symbols feature the spectral signatures of a variety of green leaves and needles (open diamond), bare soils (full circles) and snow (asterisks).

ground, respectively. The comparison between our estimates of the fraction of absorbed radiation assuming ‘green’ elements only against those delivered by the operational MODIS and MISR processors is performed in the second subsection. The third subsection demonstrates the capability of the JRC-TIP to generate consistent sets of products from the MODIS and MISR derived broadband visible and near-infrared surface albedo values.

3.1. Analysis of Retrieved Parameters and Flux Time-Series

[21] Figures 2, 3 and 4 display (top left panel) the time series of the broadband visible (full circles) and near-infrared (full squares) MODIS (red color) and MISR (blue color) BHR-white sky surface albedo over sites identified as NSAOBS, YAKUTSKspas and CHEQCenter, respectively (see Table 1). On all these figures, the MODIS values are reported on day 8 of every 16-day period while the MISR values are associated with day 4 of every 8-day period. Overall, the two sets of products appear to be in good agreement, including when snow has been detected (identified by triangles on top axes), although the algorithms selected to generate these two sets of albedo values are significantly different. More detailed investigations reveal, however, that the MISR-derived values, in both the visible and near-infrared domains, tend to be slightly higher,

roughly 5 to 10% in relative terms (depending on the location), than those estimated from MODIS. These limited, although not always negligible, spectral differences and their causes have been already documented and discussed in the literature [see, e.g., *Pinty et al.*, 2004b, 2006b; *Lyapustin et al.*, 2007].

[22] The intraannual variations in BHR values (top left panels) over the three selected sites are dominated by the occurrence of snow events at the beginning and end of the year. Under such conditions, and as expected, the values in the visible domain increase dramatically and reach a level close to or even higher than those estimated in the near-infrared domain. This leads to spectral observations inverted with respect to those prevailing in the absence of snow and/or when vegetation cover and density evolve in the course of the year according to vegetation phenology [*Pinty et al.*, 2007, Figure 5]. In the vast majority of cases, the occurrence of snow provided by the MODIS indicator, is associated with large visible surface albedo values. A noticeable exception to this relationship is observed in mid-February over YAKUTSKspas where high surface albedos from MISR and MODIS suggest the presence of snow while the MODIS indicator, after re-mapping at 500 m resolution, reveals the occurrence of cloudy conditions instead.

[23] Over all studied sites, the time series in effective LAI (top right panels) exhibit smooth variability, as can be expected from the dominant vegetation type and cover, and, consequently, show that the inversion scheme is able to properly account for drastic changes in the measurement sets due to snow occurrences and associated melting events. The amplitude of the seasonal cycle over the evergreen needleleaf site NSAOBS is quite limited (see top right panel in Figure 2). By contrast, the seasonal variation is quite smooth for deciduous forest systems (see top right panel in Figures 3 and 4) and effective LAI values remain realistic even in the presence of snow. The very large unrealistic LAI values retrieved in mid-February over YAKUTSKspas are a consequence of assigning too much importance to prior information on the background spectral properties that probably turns out to be false, snow covered versus snow-free conditions. In this particular case, the MODIS snow product indicates the probable presence of clouds and the large retrieved LAI values are masking the background spectral signatures to compensate for the low background reflectance (prior values in the absence of snow). Note that relaxing the constraints on the background properties, i.e., increasing the variances in the prior covariance matrix, would, in this case, be appropriate to avoid such unrealistic changes but would also cause the uncertainties on all the retrievals to increase quite significantly. As discussed by *Pinty et al.* [2007, section 4] and given that only two spectral BHRs are available in the measurement set **d**, the inversion returns large LAI uncertainties when LAI takes values larger than approximately unity (see top right panel in Figure 4). By contrast, one can notice that LAI is retrieved quite accurately in presence of snow since, in this condition, the forest background albedo takes on spectral values whose combination in the visible, near-infrared plane indeed facilitates the estimate of LAI.

[24] Variations in the background albedo values (middle left panels) are roughly mirroring those observed in the surface albedo but with a larger spectral contrast when snow

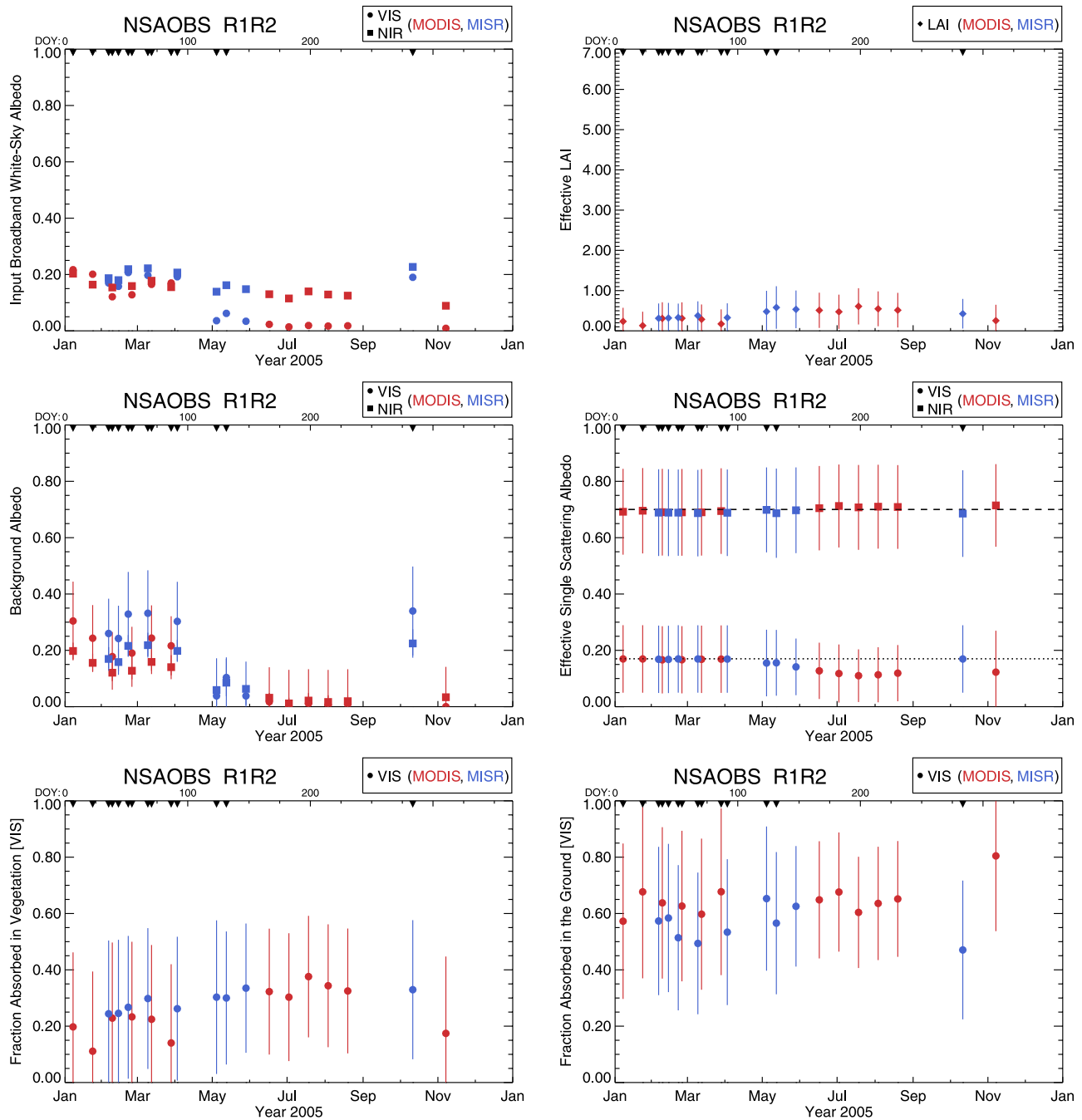


Figure 2. Time series of the surface albedo products (top left) and retrieved 2-stream model parameters and radiant fluxes over NSA OBS. MODIS (MISR) derived values are featured in red (blue) color. Products estimated in the broadband visible (near-infrared) domain are depicted with full circles (squares). Top right: effective LAI. Middle left: background albedo. Middle right: effective single scattering albedo where the dashed lines indicate the prior values. Bottom left (right): fraction of absorbed radiation in vegetation (ground) in the visible domain. Triangles on the top axis mark snow events.

occurs, i.e., the visible values are largely exceeding those retrieved in the broadband near-infrared domain. This situation then gets reversed when snow is not detected, given the strong absorption and enhanced level of leaf scattering characterizing healthy green vegetation. Over some sites, such as YAKUTSKspas for instance (middle left panel in Figure 3), the differences between the MISR and MODIS derived surface albedo products translate into

distinct sets of background albedo values, with MODIS values being lower than the corresponding ones from MISR. It thus looks like the slight bias mentioned earlier at the level of the surface albedo products translates into different solutions regarding the retrieved background properties. In general, retrievals based on MODIS products suggest darker (relatively low albedo values) and less green (relatively limited spectral contrast) forest understory than is the case

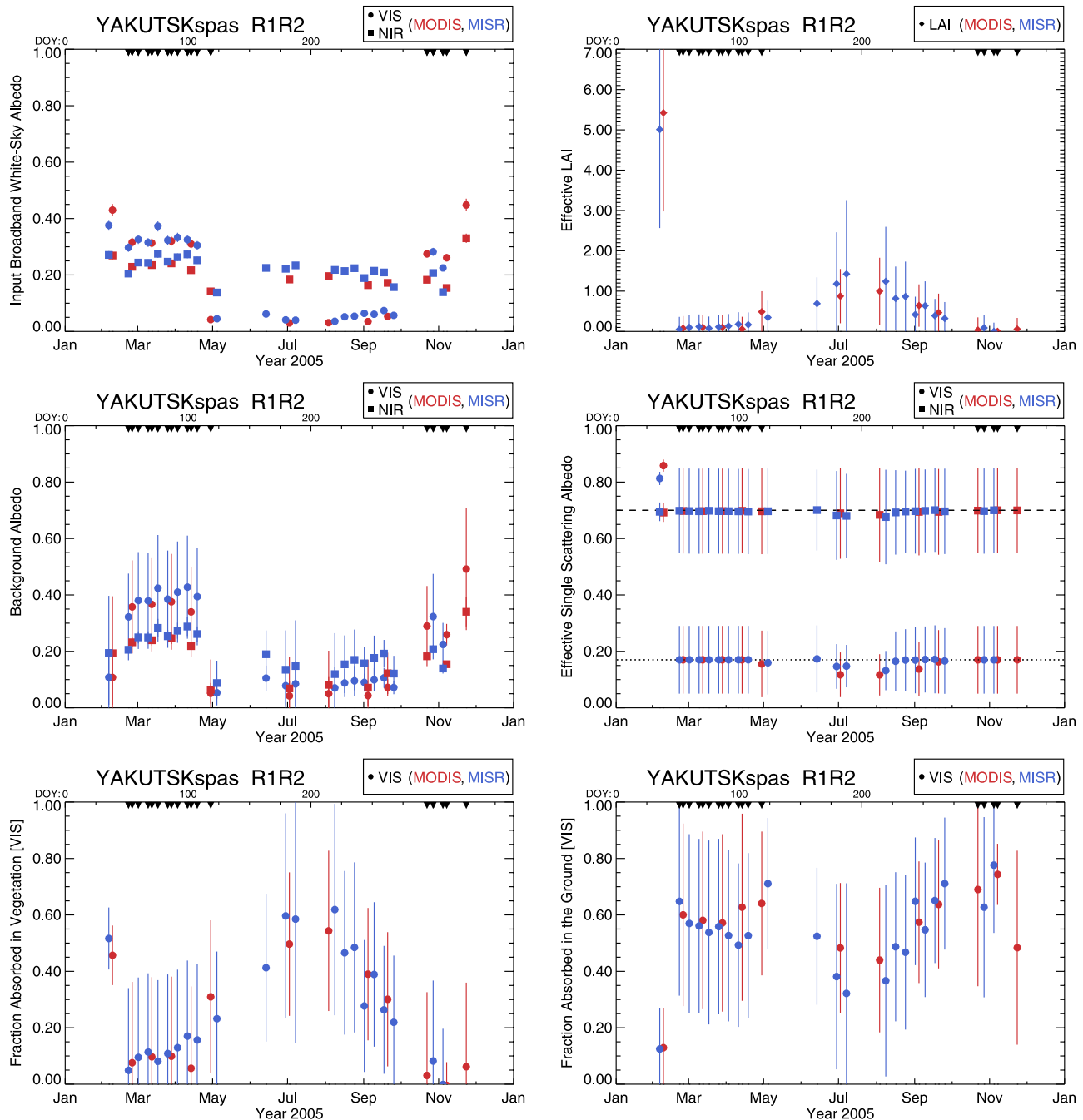


Figure 3. Time series of the surface albedo products (top left) and retrieved 2-stream model parameters and radiant fluxes over YAKUTSKspas. MODIS (MISR) derived values are featured in red (blue) color. Products estimated in the broadband visible (near-infrared) domain are depicted with full circles (squares). Top right: effective LAI. Middle left: background albedo. Middle right: effective single scattering albedo where the dashed lines indicate the prior values. Bottom left (right): fraction of absorbed radiation in vegetation (ground) in the visible domain. Triangles on the top axis mark snow events.

with MISR products. Note that this information is directly relevant to investigate the MODIS versus MISR albedo bias, since the retrieved background albedos are true values (by opposition to effective values in the sense of the radiation transfer processes) that can thus be evaluated against in situ observations.

[25] The effective single scattering albedo values (middle right panels) deviate from their priors only when the LAI

increases, that is, when the vegetation density/cover becomes high enough that leaf backscattering controls a large fraction of the measured surface albedos. This confirms earlier findings discussed by *Pinty et al.* [2007, section 4] and *Lavergne et al.* [2006]. It is, however, interesting to observe that under favorable conditions, i.e., when the uncertainty on the posteriors is smaller than that on the priors, the maximum likelihood of the single scat-

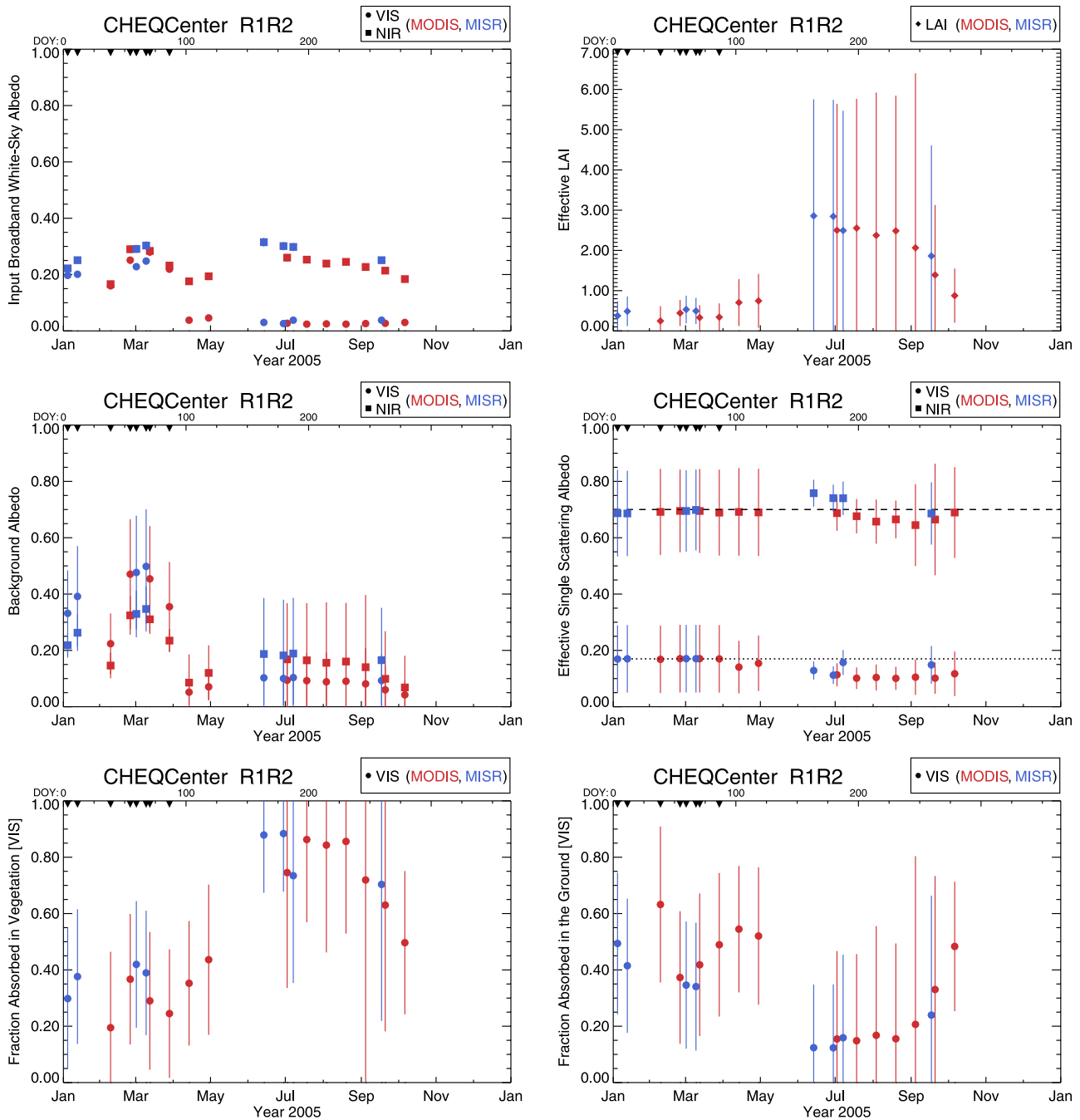


Figure 4. Time series of the surface albedo products (top left) and retrieved 2-stream model parameters and radiant fluxes over CHEQCenter. MODIS (MISR) derived values are featured in red (blue) color. Products estimated in the broadband visible (near-infrared) domain are depicted with full circles (squares). Top right: effective LAI. Middle left: background albedo. Middle right: effective single scattering albedo where the dashed lines indicate the prior values. Bottom left (right): fraction of absorbed radiation in vegetation (ground) in the visible domain. Triangles on the top axis mark snow events.

tering albedo values differ among the various studied sites: a small reduction in the visible domain only over NSA OBS, METL (not shown) and YAKUTSKspas, a reduction in both spectral domains over CHEQCenter, a reduction in the visible associated with an increase in the near-infrared domain over HESSE (not shown) and Harv (not shown). These seasonal signals appear to be associated with the dominant vegetation type, e.g., evergreen versus deciduous

forest systems. In the particular case of the mid-February albedo measurements over YAKUTSKspas underscored earlier and which generated unrealistically high LAI values with rather inaccurate background albedo estimates, the JRC-TIP also returned extremely high single scattering albedo values in the visible domain in order to fit the observations. Although this particular measurement set is not properly interpreted due to the use of inappropriate prior

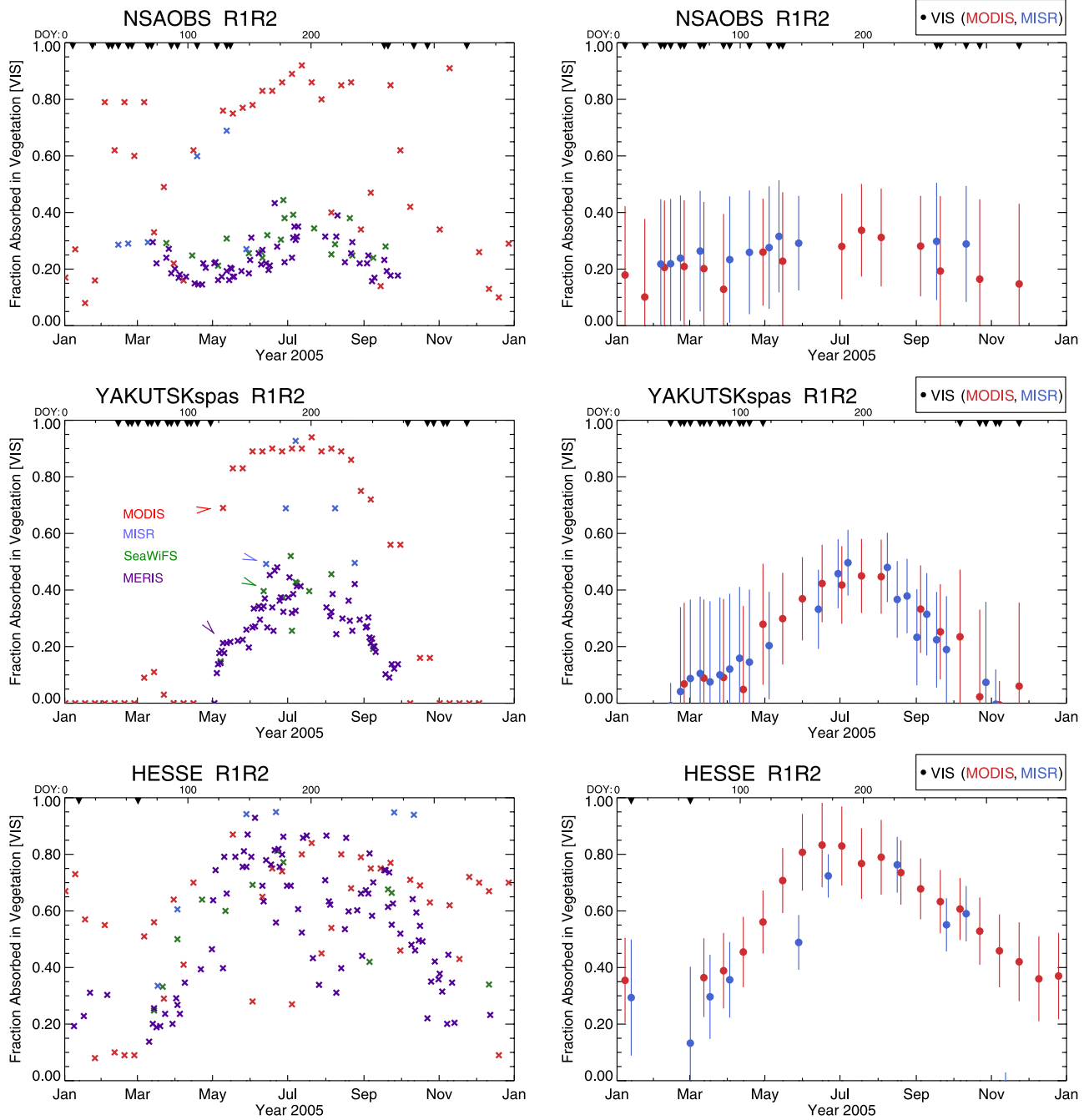


Figure 5. Time series of the fraction of absorbed radiation in vegetation by ‘green’ material only in the visible domain (FAPAR) delivered by the JRC-TIP (right panels) and those generated from major operational products (left panels) for the sites identified as NSAOBS, YAKUTSKspas and HESSE (see Table 1). The red, blue, green and violet colors are for the MODIS 8-day composite, the daily MISR, the daily JRC-SeaWiFS and MERIS operational products, respectively. Triangles on the top axis mark snow events.

knowledge, it permits us to further document the behavior of the inversion package and to illustrate the impact of inaccurately setting the elements of the prior covariance matrix. In these cases, the retrievals are strongly penalized and the inversion package returns rather large values of the cost function (equation (2)).

[26] The fraction of solar radiation absorbed by the background, $A_{bgd}(\lambda)$, is simply estimated as the fraction

of the incoming radiation which is neither reflected by the complex surface (soil background and canopy) nor absorbed in the vegetation layer:

$$\begin{aligned} A_{bgd}(\lambda) &= 1 - BHR_{sfc}(\lambda) - A_{veg}(\lambda) \\ &= T_{veg}(\lambda) (1 - r_g(\lambda)) \end{aligned} \quad (4)$$

where $A_{veg}(\lambda)$ and $BHR_{sfc}(\lambda)$ are the fractions of radiation absorbed in the vegetation layer and scattered by the surface at the top of the canopy, respectively. $T_{veg}(\lambda)$ is the total (direct + diffuse) transmission factor of incoming solar radiation, and $r_g(\lambda)$ is the soil background albedo. In the visible domain, this transmission factor is predominantly controlled by the direct/uncollided contribution that is, in fact, the extinction associated with the effective LAI values. The fluxes corresponding to A_{bgd} in the visible domain are shown on the bottom right panels of Figures 2, 3 and 4. The fluxes are varying seasonally in concert with LAI. In the near-infrared domain (not shown here), the temporal variations are somewhat dampened given that the relatively enhanced scattering by the leaves/needles with increasing LAI partly compensates for the reduction of direct radiation reaching the background: typical values over the seasons are in the range of 0.7–0.8, 0.5–0.8 and 0.2–0.6 over sites identified as NSAOBS, YAKUTSKspas and CHEQCenter, respectively.

3.2. Comparison of FAPAR Time Series From Different Sources

[27] Figure 5 compares, for the sites identified as NSAOBS, YAKUTSKspas and HESSE (see Table 1), the FAPAR time series delivered by the JRC-TIP (right panels) to operational products available from major agencies (left panels), with omission of their expected uncertainty ranges for sake of readability of the figure. The posterior two-stream model parameter values used to estimate the FAPAR are those retrieved using the ‘green’ leaf scenario (see Table 2) and these mean values (full circles) are shown here for an isotropic diffuse solar irradiance, together with the standard deviations (vertical bars) associated with the PDF of the retrieved values inferred from the posterior covariance matrix. The operational FAPAR products (left panels) correspond to the MODIS 8-day composite (red crosses) [Myneni *et al.*, 2002], the daily MISR (blue crosses) [Knyazikhin *et al.*, 1998], the daily JRC-SeaWiFS (green crosses) [Gobron *et al.*, 2006] and the daily MERIS (violet crosses) [Gobron *et al.*, 1999, 2007] products, respectively. This figure reveals that:

[28] 1. Time series of the FAPAR values estimated from the JRC-TIP (right panels) exhibit smooth variability (by contrast to those characterizing the input albedos), as expected from the dominant vegetation types and covers. This demonstrates that our procedure is able to seamlessly account for drastic changes in the surface albedo measurement sets due to snow related events in the winter and spring seasons.

[29] 2. The observed differences between the MODIS versus the MISR based results of the mean values are attributed to the slight differences in the input BHR albedo values. In the vast majority of cases these differences remain within the uncertainty range of our estimates.

[30] 3. The amplitude in the seasonal variation, as retrieved from the JRC-TIP considering ‘green’ elements only, over the evergreen needleleaf NSAOBS site is quite limited and the FAPAR values remain within approximately 0.10 and 0.40. The seasonal changes observed at other locations correspond to the variations expected to occur over deciduous sites, with a decidedly larger amplitude in the case of the broadleaf, (0.2 to 0.9) compared to the needleleaf site, (0.0 to 0.5).

[31] 4. The FAPAR values retrieved by the JRC-TIP using the MODIS and MISR albedos are in remarkable agreement with those delivered by the MERIS (violet crosses) operational processor as well as those generated from SeaWiFS (green crosses) using the JRC-FAPAR algorithm. The differences between the FAPAR estimated under diffuse irradiance (right panels) and those estimated at the Sun angle prevailing during the MERIS/SeaWiFS acquisitions were found to be negligible, in fact falling well within the uncertainty range of the retrievals, for the studied sites. A closer investigation of the MERIS daily operational product for HESSE in the summer 2005 season reveals that the unrealistic low values are associated with local clear sky conditions occurring in the middle of large cloud systems which are probably contaminating the estimates.

[32] 5. The FAPAR values generated by the operational MODIS (red crosses on the left panels) processor exhibit a rather large and probably unrealistic intraannual variability with 8-day composite values ranging, for instance, from about 0.1 to 0.9 over the evergreen needleleaf site of NSAOBS. The seasonal amplitude is about twice larger than the one derived in this study in the case of the deciduous needleleaf site of YAKUTSKspas. The large temporal variability observed at the beginning and end of the year over HESSE is not credible and this contrasts quite strongly with the reasonable smooth variations derived here.

[33] 6. The values delivered by the MISR (blue crosses) operational processor also exhibit a large temporal variability, including rather abrupt rises to high values in spring that can hardly be linked to any known biophysical process in such vegetation types. Moreover, the operational algorithm seems to deliver fewer FAPAR values than is currently returned, with documented uncertainties, by the JRC-TIP, for instance over the site of YAKUTSKspas.

[34] The comparison of FAPAR (and LAI) values delivered by the JRC-TIP when switching the priors from the baseline to the ‘green’ leaf scenario permits us to evaluate the contribution to the absorption process that is due to the ‘non-green’, probably woody, elements of the canopies. Such a comparison, which can be performed visually (bottom left panels on Figures 2 and 3 against right panels on Figure 5) over the evergreen (deciduous) needleleaf site of NSAOBS (YAKUTSKspas), confirms that the absorption by ‘green’ elements alone in the visible domain underestimates the total absorption by an amount which, although generally small, is depending on the dominant vegetation type and LAI values.

3.3. Comparing JRC-TIP Retrievals Based on MODIS and MISR Albedos

[35] Figure 6 displays the comparison between the MODIS and MISR LAI values derived with our inverse package (top panels with log scale axes), the fraction of absorbed flux in the vegetation layers (middle panels) and the ground layers (bottom panels), respectively, for the six sites listed in Table 1 and identified here with a color code. The latter two fluxes are those corresponding to perfectly isotropic illumination conditions. The left (right) panels show results obtained using low (high or ‘green’ like scenario) constraints on the effective single scattering albedo (see Table 2). The 1σ uncertainty range associated with these retrievals is featured as dotted lines.

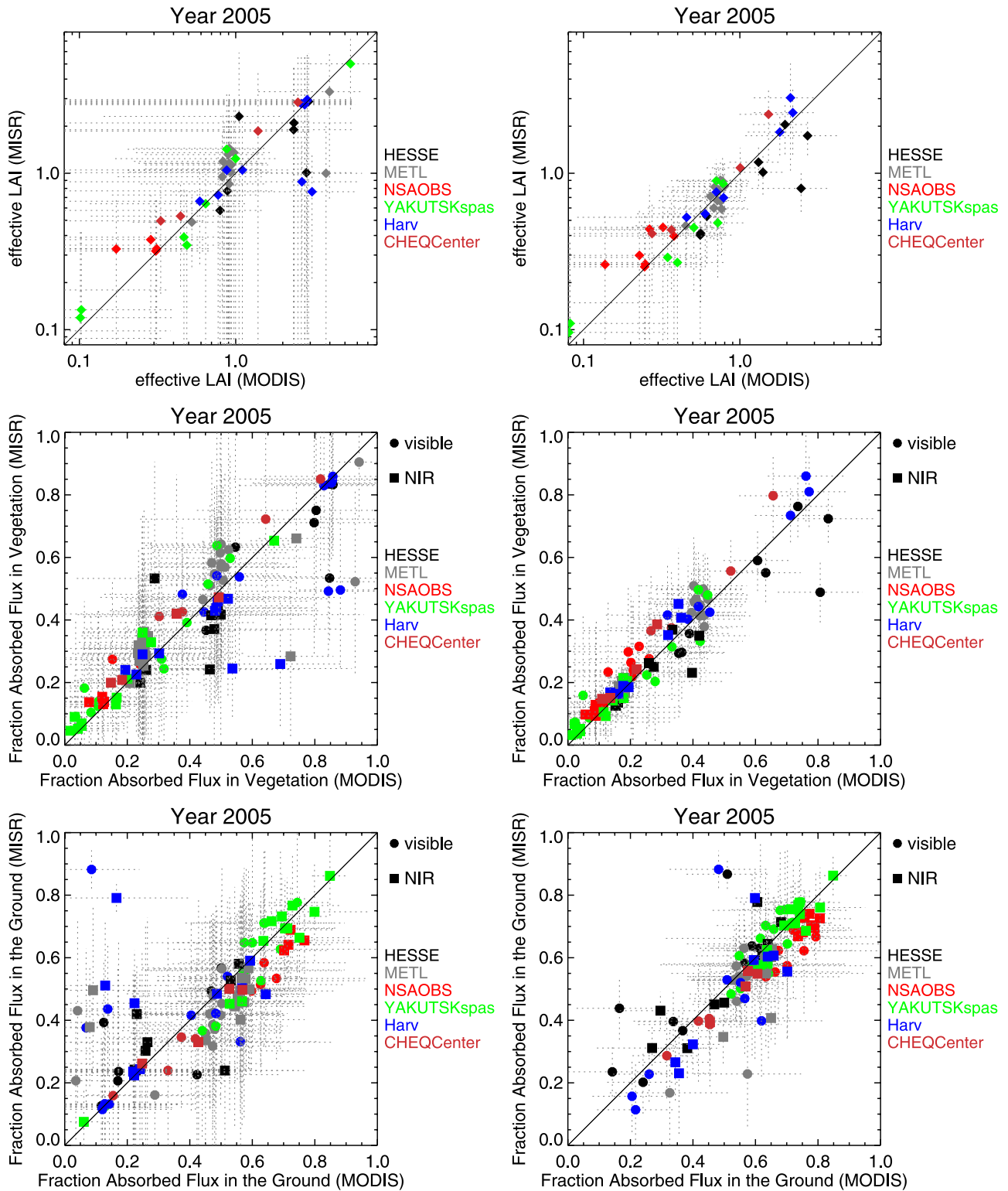


Figure 6. Comparison of the JRC-TIP retrievals using MODIS and MISR visible (full circles) and near-infrared (full squares) BHRs. The left and right hand panels show results obtained using low (see Table 2) and high ('green') constraints on the effective single scattering albedos. Different colors correspond to different sites. The dotted lines indicate the 1σ uncertainty range associated with these retrievals.

[36] The two noticeable outcomes from this figure relate to 1) the very good agreement between these retrieved products when applying the JRC-TIP algorithm to the MODIS and MISR albedos over a large ranges of conditions and 2) the significant reduction in uncertainties, i.e., smaller variance values along the diagonal of the covariance matrix, associated with these estimates when adopting the 'green' leaf scenario (right panels). The retrievals deviating most from the one-to-one lines are usually associated with a significant probability of contamination by partly cloudy conditions, e.g., over Harv and HESSE in the summer season, and/or the confusion between snow and cloud occurrence at high latitude locations in winter and spring seasons. An additional source of deviations between the two series of retrievals is caused by differences in the spectrally integrated albedo measurement sets. It is noteworthy that the MODIS albedo values, derived from an algorithm based on sequential accumulation, are associated with 16-day periods unlike those instantaneous from MISR which are thus valid for one specific day within a given 16-day period.

[37] The good agreement between the JRC-TIP based estimates of the ground flux derived from MODIS and MISR is especially noticeable given that this latter flux incorporates joint assessments of the radiation transmitted through the vegetation canopy layer and the albedo of the background. It thus appears that any remaining differences and biases between the MODIS and MISR albedo values may only mildly impact (in the sense that the differences in the mean PDF values remain within the 1σ estimated uncertainty) high level flux products such as, for instance, the absorbed flux in the ground.

4. Conclusions

[38] This series of examples, addressing rather difficult geophysical situations such as those associated with snow events in tall vegetation canopy environments, illustrates the potential for deriving consistent sets of surface products (both state variables and fluxes) across different space platforms, e.g., the FAPAR values derived from the Terra albedo products and the MERIS/SeaWiFS instruments. It was shown that, in addition, the availability of a snow indicator is beneficial to the analysis of products generated under winter and early spring seasons, especially at high latitudes. The high level of consistency found between these fluxes is promising for future applications and suggests the design of integrated systems capable of assimilating a variety of sources of information on land surfaces.

[39] The capability of our inversion procedure to account properly for the temporal changes in the radiative properties of forest backgrounds while maintaining smooth temporal profiles in LAI has been demonstrated. The background albedo values are capturing most of the variations observed in the surface albedo at the top of the canopy but with a larger spectral contrast under occurrence of snow, i.e., the visible values get much larger than those retrieved in the broadband near-infrared domain. This ensemble of results illustrates our ability to separate the radiation transfer processes controlling the relative contributions of the vegetation layer and its background.

[40] These results also suggest that the slight differences existing between the input MODIS and MISR surface albedo

values do not generally translate into significantly discernible signatures on major parameters such as the effective LAI and the fluxes absorbed in the vegetation layers and the underlying backgrounds. In all cases studied here, the time series of the retrieved parameters and fluxes are smooth (except under a few specific but well-documented instances); they exhibit much less variability than those generated by the operational MODIS and MISR algorithms. This finding confirms results from the earlier investigation conducted by *Pinty et al.* [2007] over locations characterized by vegetation types different from those considered here.

[41] It is worthwhile emphasizing that the JRC-TIP fulfills the stringent requirements imposed by operational processing, including reliability, robustness and computer efficiency. Its implementation remains quite flexible and allows its operation using various sets of input measurements, e.g., albedo and FAPAR flux values, either jointly or one at a time. Further efforts will be addressing 1) the evaluation of the retrievals, for instance by assessing albedos and transmitted fluxes over selected instrumented sites and 2) the assimilation of remote sensing flux values in a time-dependent approach which should help to further reduce the uncertainties in the retrievals.

[42] **Acknowledgments.** The authors gratefully acknowledge the contribution from M. Robustelli and F. Mélin. R. Suzuki kindly provided the authors with detailed information about the site of YAKUTSKspas. The authors would like to thank the providers of the remote sensing data sets needed to perform this research. The MISR products were obtained from the NASA Langley Research Center Atmospheric Sciences Data Center. The MODIS products were obtained from the National Snow and Ice Data Center and the NASA Land Processes Distributed Active Archive Centers. The authors also thank the Ocean Biology Processing Group and the Distributed Active Archive Center at the NASA Goddard Space Flight Center for the distribution of the SeaWiFS data. The authors are also grateful to Brockman Consult (Geesthacht, Germany), ACRI (Sophia Antipolis, France) and ESA-ESRIN for their dedicated help and support. This research was performed in the Global Environment Monitoring unit of the Institute for Environment and Sustainability at the DG Joint Research Centre, an institution of the European Commission.

References

- Avissar, R., and M. M. Verstraete (1990), The representation of continental surface processes in mesoscale atmospheric models, *Rev. Geophys.*, *28*, 35–52.
- Betts, A. K. (2007), Coupling of water vapor convergence, clouds, precipitation, and land-surface processes, *J. Geophys. Res.*, *112*, D10108, doi:10.1029/2006JD008191.
- Chi, H. (2003), Practical atmospheric correction of NOAA-AVHRR data using the bare-sand soil line method, *Int. J. Remote Sens.*, *24*, 3369–3379.
- Dickinson, R. E. (1983), Land surface processes and climate-surface albedos and energy balance, *Adv. Geophys.*, *25*, 305–353.
- Dickinson, R. E., A. Henderson-Sellers, P. J. Kennedy, and M. F. Wilson (1986), Biosphere Atmosphere Transfer Scheme (BATS) for the NCAR Community Climate Model, *Technical Note TN275+STR*, National Center for Atmospheric Research.
- Enting, I. G., C. M. Trudinger, and R. J. Francey (1995), A synthesis inversion of the concentration and $\delta^{13}\text{C}$ of atmospheric CO_2 , *Tellus, Ser. B*, *47*, 35–52.
- Giering, R., and T. Kaminski (1998), Recipes for adjoint code construction, *ACM Trans. Math. Software*, *24*, 437–474.
- Gobron, N., B. Pinty, M. M. Verstraete, and Y. Govaerts (1999), The MERIS Global Vegetation Index (MGVI): Description and preliminary application, *Int. J. Remote Sens.*, *20*, 1917–1927.
- Gobron, N., et al. (2006), Evaluation of FAPAR products for different canopy radiation transfer regimes: Methodology and results using Joint Research Centre products derived from SeaWiFS against ground-based estimations, *J. Geophys. Res.*, *111*, D13110, doi:10.1029/2005JD006511.
- Gobron, N., B. Pinty, F. Mélin, M. Taberner, M. Verstraete, M. Robustelli, and J.-L. Widowski (2007), Evaluation of the MERIS/ENVISAT FAPAR product, *Adv. Space Res.*, *39*, doi:10.1016/j.asr.2006.02.048.

- Gower, S. T., and J. M. Norman (1991), Rapid evolution of leaf area index in conifer and broad-leaf plantations, *Ecology*, **72**, 1896–1900.
- Hall, D. K., J. L. Foster, D. L. Verbyla, A. G. Klein, and C. S. Benson (1998), Assessment of snow cover mapping accuracy in a variety of vegetation cover densities in central Alaska, *IEEE Trans. Geosci. Remote Sens.*, **66**, 129–137.
- Hosgood, B., S. Jacquemoud, G. Andréoli, J. Verdebout, G. Pedrini, and G. Schmuck (1995), Leaf Optical Properties Experiment (LOPEX' 93), *Technical Report EUR 16095 EN*, EC Joint Research Centre.
- Jacquemoud, S., and F. Baret (1990), PROSPECT: A model of leaf optical properties spectra, *Remote Sens. Environ.*, **34**, 75–91.
- Jonckheere, L., S. Fleck, K. Nackaerts, B. Muys, P. Coppin, M. Weiss, and F. Baret (2004), Review of methods for in situ leaf area index determination. Part theories I. sensors and hemispherical photography, *Agric. For. Meteorol.*, **121**(1), 19–35.
- Knyazikhin, Y., J. V. Martonchik, D. J. Diner, R. B. Myneni, M. M. Verstraete, B. Pinty, and N. Gobron (1998), Estimation of vegetation canopy leaf area index and fraction of absorbed photosynthetically active radiation from atmosphere-corrected MISR data, *J. Geophys. Res.*, **103**, 32,239–32,256.
- Lavergne, T., M. Voßbeck, B. Pinty, T. Kaminski, and R. Giering (2006), Evaluation of the 2-stream model inversion package, *EUR Report No. 22467 EN*, Joint Research Centre, Institute for Environment and Sustainability.
- Lyapustin, A., Y. Wang, R. Kahn, J. Xiong, A. Ignatov, R. Wolfe, A. Wu, B. Holben, and C. Bruegge (2007), Analysis of MODIS-MISR calibration differences using surface albedo around aeronet sites and cloud reflectance, *Remote Sens. Environ.*, **107**, 12–21.
- Martonchik, J. V., D. J. Diner, B. Pinty, M. M. Verstraete, R. B. Myneni, Y. Knyazikhin, and H. R. Gordon (1998), Determination of land and ocean reflective, radiative, and biophysical properties using multiangle imaging, *IEEE, Trans. Geosci. Remote Sens.*, **36**, 1266–1281.
- Meador, W. E., and W. R. Weaver (1980), Two-stream approximations to radiative transfer in planetary atmospheres: A unified description of existing methods and new improvements, *J. Atmos. Sci.*, **37**, 630–643.
- Myneni, R. B., et al. (2002), Global products of vegetation leaf area and fraction absorbed PAR from year one of MODIS data, *Remote Sens. Environ.*, **83**, 214–231.
- Pinty, B., N. Gobron, J.-L. Widlowski, T. Lavergne, and M. M. Verstraete (2004a), Synergy between 1-D and 3-D radiation transfer models to retrieve vegetation canopy properties from remote sensing data, *J. Geophys. Res.*, **109**, D21205, doi:10.1029/2004JD005214.
- Pinty, B., et al. (2004b), Intercomparison of surface albedo products from various spaceborne sensors, in *Proceedings of the Workshop on Inter-Comparison of Large Scale Optical and Infrared Sensors, ESA ESTEC, ESA ESTEC, Noordwijk, The Netherlands*, 12–14 October 2004.
- Pinty, B., T. Lavergne, R. E. Dickinson, J.-L. Widlowski, N. Gobron, and M. M. Verstraete (2006a), Simplifying the interaction of land surfaces with radiation for relating remote sensing products to climate models, *J. Geophys. Res.*, **111**, D02116, doi:10.1029/2005JD005952.
- Pinty, B., et al. (2006b), MODIS/Meteosat/MISR surface albedo comparison results, in *Proceedings of the 4th International Workshop on Multiangular Measurements and Models*, CSIRO, Sydney, Australia, 20–24 March 2006.
- Pinty, B., T. Lavergne, M. Voßbeck, T. Kaminski, O. Aussedat, R. Giering, N. Gobron, M. Taberner, M. M. Verstraete, and J.-L. Widlowski (2007), Retrieving surface parameters for climate models from MODIS and MISR albedo products, *J. Geophys. Res.*, **112**, D10116, doi:10.1029/2006JD008105.
- Pitman, A. (2003), The evolution of, and revolution in, land surface schemes designed for climate models, *Int. J. Climatol.*, **23**, 479–510.
- Rautiainen, M., P. Stenberg, T. Nilson, and A. Kuusk (2004), The effect of crown shape on the reflectance of coniferous stands, *Remote Sens. Environ.*, **89**, 41–52.
- Rich, P. M. (1990), Characterizing plant canopies with hemispherical photographs, instrumentation for studying vegetation canopies for remote sensing in optical and thermal infrared regions, *Remote Sens. Rev.*, **5**, 13–29.
- Schaaf, C. B., et al. (2002), First operational BRDF, albedo and nadir reflectance products from MODIS, *Remote Sens. Environ.*, **83**, 135–148.
- Sellers, P. J. (1985), Canopy reflectance, photosynthesis and transpiration, *Int. J. Remote Sens.*, **6**, 1335–1372.
- Sellers, P. J., et al. (1997), Modeling the exchanges of energy, water, and carbon between continents and the atmosphere, *Science*, **275**, 502–509.
- Tarantola, A. (1987), *Inverse Problem Theory, Methods for Data Fitting and Model Parameter Estimation*, 630 pp., Elsevier Science, New York.
- Verstraete, M. M. (1989), Land surface processes in climate models: Status and prospects, in *Climate and the Geosciences: A Challenge for Science and Society in the 21st Century*, edited by A. Berger, S. H. Schneider, and J. C. Duplessy, pp. 321–340, Kluwer Academic Publishers, Dordrecht.
- Viterbo, P., and A. K. Betts (1999), Impact on ECMWF forecasts of changes to the albedo of the boreal forests in the presence of snow, *J. Geophys. Res.*, **104**, 27,803–27,810, doi:10.129/1998JD200076.
- Widlowski, J. L., et al. (2006), The third Radiation transfer Model Inter-comparison (RAMI) exercise: Documenting progress in canopy reflectance modelling, *J. Geophys. Res.*, **112**, D09111, doi:10.1029/2006JD007821.

O. Aussedat, N. Gobron, T. Lavergne, B. Pinty, M. Taberner, M. M. Verstraete, and J.-L. Widlowski, European Commission, DG Joint Research Centre, Institute for Environment and Sustainability, Global Environment Monitoring Unit, TP 440, via E. Fermi, I-21020, Ispra (VA), Italy. (bernard.pinty@jrc.it)

R. Giering, T. Kaminski, and M. Voßbeck, FastOpt, Schanzenstrasse 36, D-20357, Hamburg, Germany.